ISBN(softcover): 978-3-0364-0997-9 ISBN(eBook): 978-3-0364-1997-8

Table of Contents

Key Engineering Materials
ISSN: 1662-9795, Vol. 1047, pp 31-40
doi:10.4028/p-3Ka8Ao

Submitted: 2025-12-15
Revised: 2026-02-20
Accepted: 2026-02-25
Online: 2026-04-13

Laser Powder Bed Fusion of INCONEL® 625: Guidelines for Robust Parameter Selection toward Optimal Quality Parts

Gabriele Locatelli[1,a*], Mariangela Quarto[1,b], Sara Bocchi[1,c], Cristian Cappellini[1,d] and Gianluca D'Urso[1,e]

[1]Department of Management, Information and Production Engineering, University of Bergamo, Via Pasubio 7/b, 24044 Dalmine, BG, Italy

[a*]gabriele.locatelli@unibg.it, [b]mariangela.quarto@unibg.it, [c]sara.bocchi@unibg.it, [d]cristian.cappellini@unibg.it, [e]gianluca.d-urso@unibg.it

[*]Corresponding author

Keywords: additive manufacturing, powder bed fusion, inconel 625, process optimization.

Abstract. Producing INCONEL® 625 (IN625) components by laser powder bed fusion (PBF-LB) demands a careful selection of process parameters to concurrently ensure high densification, stable microstructural features, and adequate surface integrity. Previous studies investigated the isolated effect of these parameters or narrow volumetric energy density (*VED*) ranges, albeit without offering indications on how to simultaneously optimize surface roughness, microhardness, and density. Furthermore, the validity of *VED* as an input for process optimization is still debated. The present study offers a systematic exploration of the laser power–scan speed (*P–v*) space over a wide VED interval (33–400 J/mm³) to identify stable and robust process regimes for PBF-LB of IN625. Cylindrical samples built according to dissimilar *P–v* combinations reveal an extended process window where the properties of interest remain well balanced. Within this region, surface roughness below 10 μm, microhardness near 300 HV_1, and relative density over 99.5% were consistently achieved. Furthermore, distinct *P–v* combinations sharing the same *VED* value were confirmed to produce markedly different results, underscoring the limitations of *VED* as a predictive descriptor. The findings allowed to establish quantitative guidelines for selecting robust *P–v* conditions, offering a practical foundation for future data-driven or physics-informed multi-objective process optimisation of PBF-LB IN625.

Introduction

Nickel-based superalloys, and specifically INCONEL® 625 (IN625), are fundamental materials for high performance applications due to their excellent mechanical strength, good fatigue properties, hot corrosion resistance, and stability at temperatures approaching 1000 °C [1,2]. Owing to such properties, on one side, IN625 is widely used especially for critical, high-temperature and high-pressure applications in harsh aerospace, marine, and chemical processing environments [3]. On the other side, the same characteristics make its processing through traditional technologies a continuous challenge both in terms of cost and feasibility. [4].

Metal additive manufacturing (MAM) thus emerges a compelling alternative to traditional manufacturing processes, as it offers high flexibility for complex part fabrication, as well as shorter production time and lower material waste [5]. Among MAM technologies, Laser Powder Bed Fusion (PBF-LB) emerges as a disruptive technology for processing IN625 enabling geometric complexity, refined microstructures and reduced material waste that were previously not possible [6]. However, translating these advantages into industrial-grade repeatability and process qualification remains highly challenging. PBF-LB process is inherently sensitive to the variation in laser power, scan speed and energy input. Small deviations may trigger the formation of lack-of-fusion (LOF) and keyhole pores, cracks, balling and poor interlayer consolidation, which negatively affect the quality of as-built parts in terms of density, surface finish, and mechanical properties [4]. For industries operating under strict safety and reliability requirements, such variability represents a critical barrier for the adoption.

The optimization of the PBF-LB process therefore relies primarily on tuning the laser power (P) and scanning speed (v) parameters, as they primarily determine the local energy input delivered to the powder bed. Hatch distance (h) and layer thickness (t) also govern the stability of the melting process by controlling melt track overlaps and heat accumulation. Volumetric energy density (*VED*), defined according to Eq. (1), is also adopted for PBF-LB process optimization. Indeed, *VED* represents a simplified, yet practical indicator for correlating process conditions with key as-built properties such as relative density, surface roughness and microhardness [7].

$$VED = P/(v \cdot h \cdot t). \quad (1)$$

Despite significant advancements reported in the literature on PBF-LB of IN625, current knowledge does not yet provide a robust, generalizable, and multi-objective guidelines for ensuring consistent performance regardless of machines, operators, or production environment. Previous experimental studies are focused on isolated quality indicators and restrict the analysis to narrow energetic range, otherwise are relied on the definition of optimal *VED* as a synthetic descriptor of process behaviour, despite it is well-known its limitations in describing the physics of the melt pool. As summarized in Table 1, these constraints hinder the definition of an industry-relevant process window able of ensuring high density, controlled surface integrity, and stable mechanical response across a wide parameter space.

Table 1. Summary of previous methodologies and authors' proposal.

Focus and reference	Proposed methodology
Only one quality indicator at a time is analysed [8–11]	Concurrent evaluation of porosity, surface roughness and microhardness under controlled *P–v* conditions
Only narrow *VED* ranges are explored (~60–180 J/mm³) [12–16]	Systematic exploration of an extended *VED* window (33–400 J/mm³)
Parameter effects are studied individually, not as combined *P–v* interactions [9,14,17]	Quantitative analysis of *P–v* interaction to identify stable and reproducible operating domains
The predictive reliability of *VED* is not assessed [8–17]	Critical evaluation of *VED* as process descriptor

In this context there is an increasing industrial demand of reliable, transferable and physics-consistent criteria able to support the process qualification, certification workflow, and the scale-up of AM processes with high value material. To meet the industrial needs, it is not enough to identify a specific set of optimal parameters; it is necessary to define a stable process domain that is clearly separated from the defect-inducing regions and supported by a strong methodology rigorous enough to be integrated in digital twin, predictive models, and monitoring systems. Only by this vision, it will be possible to push the technology beyond the mere laboratory optimization and bring it closer to a medium-high Technology Readiness Level (TRL), where robustness, repeatability and multiplatform applicability become essential requirements.

Establishing robust guidelines for process-parameter selection is therefore essential to ensure consistent part quality, reduce variability, and improve reproducibility in industrial settings. Therefore, the present study provides a comprehensive and systematic exploration of the *P–v* parameter space, aiming to the definition of a robust window for processing IN625. By investigating the combined influence of laser power and scan speed over an extended *VED* range, the study identifies the most stable and repeatable operating regimes to concurrently optimise surface roughness, microhardness, and densification. Furthermore, this work also offers a critical assessment of whether *VED* can adequately capture process behaviour. Overall, the present study proposes quantitative guidelines for a thoughtful selection of process parameters, establishing an empirical

foundation for future optimization frameworks and in-process monitoring tools supporting the production of IN625 components with superior density and improved metallurgical quality by PBF-LB processing.

This study provides the first systematic mapping of the *P–v* space for IN625 across a wide energetic interval, delivering actionable guidelines and experimentally demonstrating the non-uniqueness of VED-based optimization.

Materials and Methods

Commercially available gas-atomized IN625 powder was used in this study characterized by a chemical composition compliant with the ranges specified by the relevant ASTM/AMS standards for Ni-alloys. The particle size distribution (PSD) was assessed by means of laser diffraction analysis. The PSD curves and characteristic D10, D50, and D90 diameter percentiles are reported in Fig. 1.

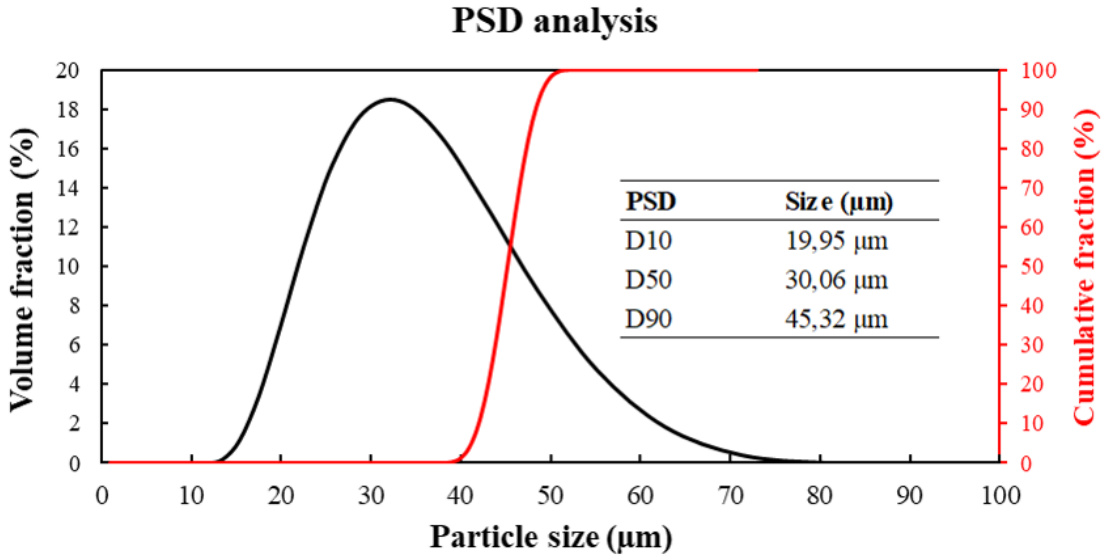

Fig. 1. PSD distribution and diameter quantiles of the IN625 powder.

To systematically capture the influence of process parameters on part quality, a Design of Experiment (DoE) was defined by varying the laser power (*P*) and scan speed (*v*), as they directly affect melt pool stability and defect formation. Specifically, *P* was varied over five levels (100–150–200–250–300 W), while *v* was varied over four levels (500–1000–1500–2000 mm/s). To minimize disturbing factors, hatch distance and layer thickness were fixed to 50 µm and 30 µm, respectively. The DoE was thus designed as a parametric map spanning twenty (20) low to high *VED* inputs ranging from 33 to 400 J/mm^3, aiming to include both under- and over-melting conditions.

As depicted in Fig. 2, cylindrical specimens (10 mm diameter and 6 mm thickness) were fabricated in a single build job using a laser powder bed fusion machine equipped with a 300W laser (Print Genius 150 by Prima Additive). The build plate was preheated to 80 °C and 5 mm-width stripe scanning strategy with 67° inter-layer rotation was adopted. The PBF-LB process was carried out under Argon gas atmosphere, keeping the oxygen level below 0.1% to prevent oxidation.

The printed specimens were analysed in the as-built condition. The average surface roughness (Sa) was assessed through 3D optical profilometry (focus variation technique, 2×2 stitching with 20% overlapping) according to the ISO 25178 standard (S-Neox by Sensofar). For each specimen, three measurements were acquired on different portions of the top surface and results were averaged for accuracy. The samples were then separated from the build platform via W-EDM. After metallographic preparation with SiC emery paper up to 1200 grits, the top surface of each specimen was subjected to Vickers testing according to the ASTM E92-17 standard. A 1000 gf load was applied for 15 s and microhardness values (HV_1) were determined as the average of five indentations. The specimens were subsequently cut parallel to the build direction via W-EDM. The mounted samples were then grinded with SiC emery paper up to 4000 grit and polished with 1 µm diamond suspension.

High-resolution images of the polished cross-sections were captured at 100× magnification using a digital optical microscope. The optical micrographs (OM) where then analysed with the ImageJ software to determine the relative density (ρ_{rel}) and characterize the porosity of each specimen.

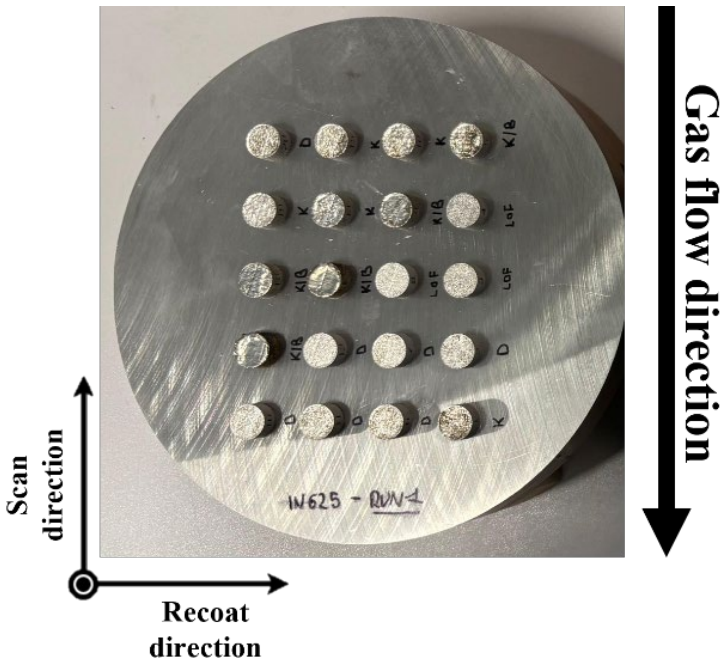

Fig. 2. Layout of the as-built IN625 cylindrical specimens on the build platform.

Results and Discussion

The combined influence of *P* and *v* on the surface texture, microhardness, and densification of IN625 processed by PBF-LB is illustrated by the graphs in Fig. 3.

Fig. 3a shows that high surface roughness is typically achieved by increasing the scanning speed for a selected laser power. Such an outcome is compatible with the formation of surface undulations rising due to unstable, irregular melt tracks and partially melted particles [18]. Interestingly, systematically higher Sa (12.4–17.4 μm) resulted from *P* = 100 W processing compared to other laser power levels used in this study. On the contrary, the roughness appears to depend mostly on the choice of the scanning speed for medium-to-high laser power (150–300 W), with values of v (500–1000 mm/s) allowing to achieve Sa values lower than 10 μm. As illustrated in Fig. 3b, microhardness in the 280–320 HV_1 range was consistently achieved. Such values are consistent with the existing literature and can be attributed to the extremely fine dendritic and columnar microstructures developed by IN625 under PBF-LB process [19]. Only the 100 W–2000 mm/s combination resulted in markedly lower hardness (233 HV_1), which can be attributed to the development of LOF pores under the tested surface due to undermelting. It is interesting to note that medium-to-high laser power and scan speed over 1500 mm/s are required to stably achieve ~300 HV_1 microhardness. For relative density, Fig. 3c shows two distinct defect-prone regimes separated by a broad processing window where melting is more uniform and repeatable, as typically reported for PBF-LB processing [4]. In particular, a 100 W laser power leads to progressive density reduction as the scan speed is increased, a result that is consistent with LOF pores forming due to undermelting. Conversely, the combination of high power (250–300 W) and low scan speed (500 mm/s) is responsible for reduced densification due to the formation of unstable melt pools and keyhole porosity promoted by overmelting. A stable operating zone for achieving near-full density IN625 (ρ_{rel} ~99.9%) is observed at intermediate speeds (1000–1500 mm/s) and P > 100 W, indicating balanced melt pool dynamics and robust material consolidation.

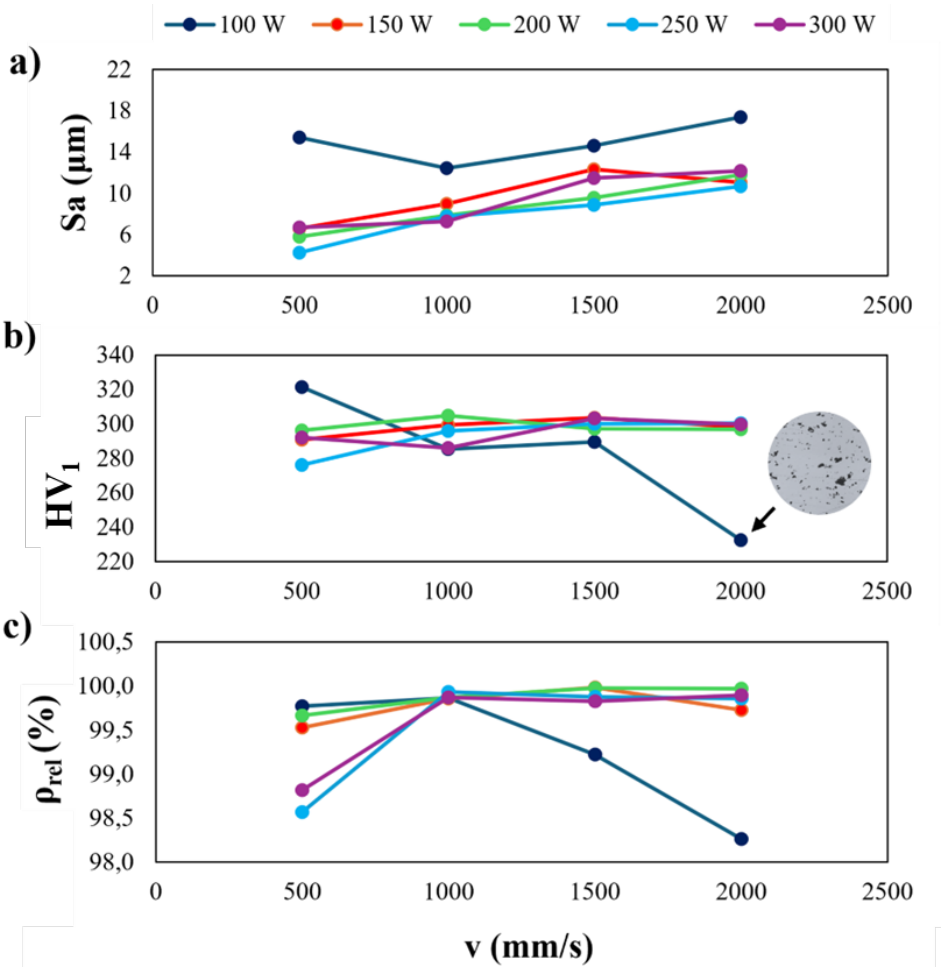

Fig. 3. (a) Surface roughness, (b) microhardness, and (c) relative density of IN625 samples as a function of scan speed for different laser powers.

While the analysis of the effect of *P* and *v* is the most rigorous method for understanding the physics of the process, analysing the effect of *VED* results to be a useful and synthetic parameter for identifying general trends of undermelting, keyholing and for comparing results with literature. Thus, surface texture, microhardness, and densification results as functions of the *VED* are summarized in Fig. 4. Sa exhibits a rapid decrease when moving from low to intermediate *VED* values, marking the transition to a stable melting regime (see Fig. 4a). However, further increases in *VED* beyond approximately 200–250 J/mm^3 do not appear to improve surface roughness significatively. On the other hand, Fig. 4b shows that microhardness remains consistently around 300 HV_1 at in the 50–267 J/mm^3. This behaviour can be associated with the refinement of dendritic structures at higher cooling rates, as reported in previous studies [20]. Finally, relative density exhibits an extended plateau for near-to-full densification between 67 and 167 J/mm^3 (see Fig. 4c). Outside this interval, the lower ρ_{rel} values stem from porosities characteristic of LOF and keyholing, as clearly illustrated by the OM in Fig. 5.

Although *VED* is widely employed as a synthetic parameter to study the PBF-LB process, its feasibility as a primary input variable for process optimisation presents intrinsic limitations. The comparison between *P*-*v* and *VED* clearly demonstrates that different combination of *P* and *v* with the same *VED* can generate dissimilar properties, highlighting the inherent limitations of *VED* as a primary optimization parameter and supporting the need for a direct evaluation of *P*-*v* parameters. As possible to observe in the area identified in Fig. 4 by a black dash-dotted ellipses, same *VED* value may lead to significantly different results in terms of surface roughness, microhardness, and densification due to being determined by different laser power-speed combinations. Such discrepancies arise due to the *VED* equation ignoring the complex physics of the melt pool such as recoil pressure, Marangoni flow, and melt-pool confinement [21].

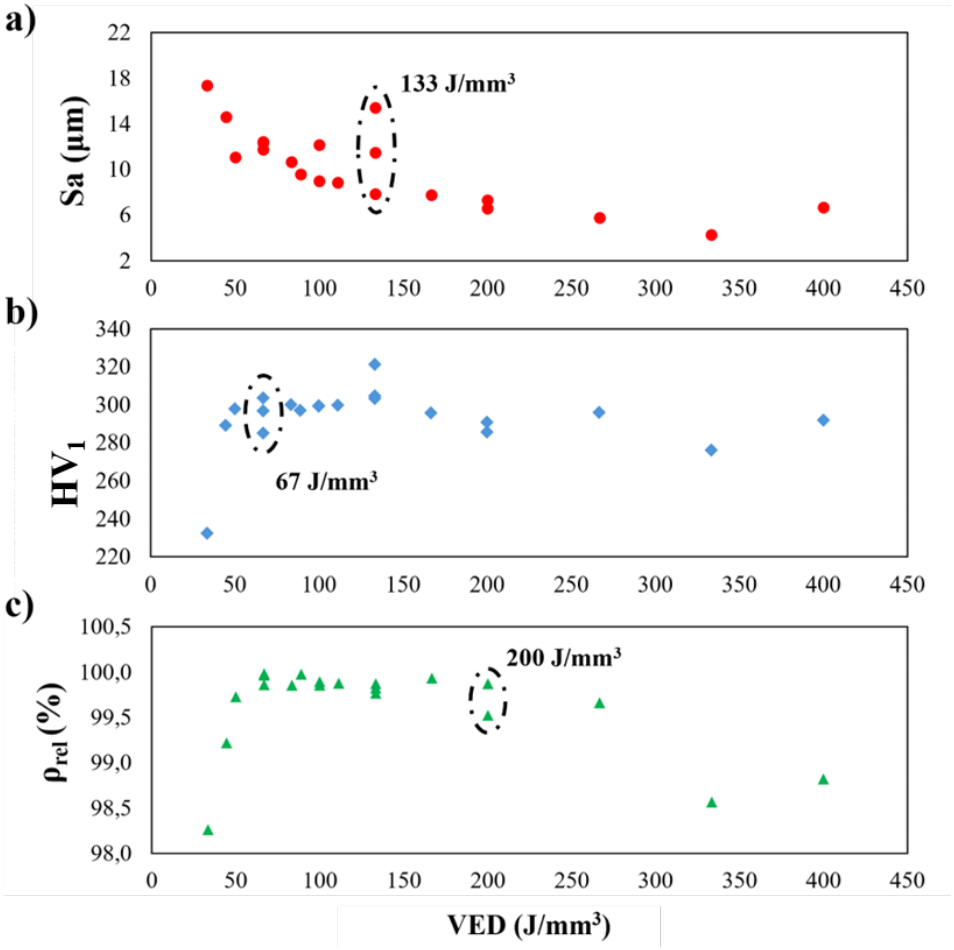

Fig. 4. (a) Surface roughness, (b) microhardness, and (c) relative density of IN625 samples as a function of volumetric energy density.

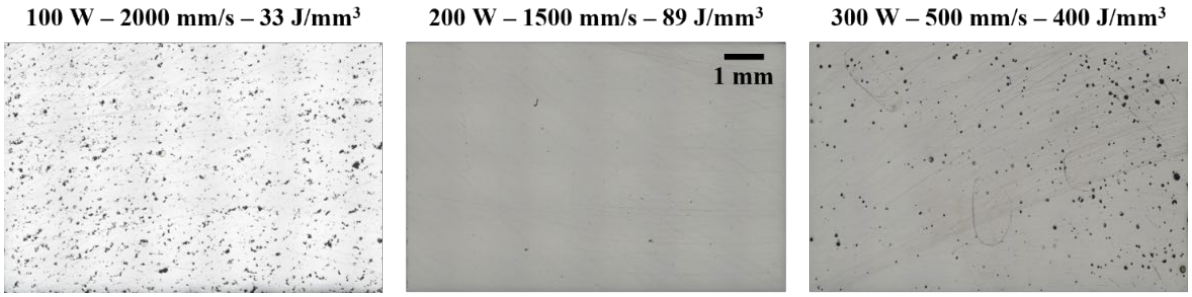

Fig. 5. OM of polished cross-sections of IN625 samples showing different densification behaviours.

The image-based porosity analysis may not reliably capture the onset of melt pool instabilities. For this reason, the cross-sections were etched by immersion in mixed acids (15 ml of HCl, 10 ml of HNO_3 and 10 ml of acetic acid) to assess melt-pool geometry. The OMs of etched cross-sections in Fig. 6 clearly depict the evolution of melt pool geometry providing a microstructural validation of the trends observed in Fig. 3 and 4, linking the variability of the measured characteristics to a specific melting condition and demonstrating how melt-pool morphology affects the surface integrity, mechanical response, and the porosity distribution.

At low VED values, high roughness and low densification were recorded, the etched cross-sections show shallow, discontinuous melt pools characteristic of undermelting. These geometries reflect poor track overlap, which explain both the increased presence of LOF defects and the formation of surface undulations generated by unstable melt-track propagation. As the VED increases into the intermediate, more stable range, the process achieves the best balance between roughness, hardness, and density, and the melt pools evolve into deeper and more uniform conduction-mode profiles. The

regular shape promotes improved interlayer bonding and reduced porosity, which aligns with the near-full densification (~99.9%) and the stable microhardness values around 300 HV_1. The refined and repeatable melt-pool geometry observed in Fig. 6 is thus a direct microstructural confirmation of the process stability inferred from the mechanical and surface measurements. At higher VED values, despite the persistence of acceptable hardness, the melt pools become progressively elongated and narrow, showing the beginning of keyhole-mode melting. These geometries are associated with vapor depression, enhanced recoil pressure, and localized instability. The keyhole morphologies correspond to the reduction in relative density observed at high power–low speed combinations, where keyhole porosity becomes more likely. This transition explains why improvements in surface roughness become stable despite the increment in the energy input: even though the melt becomes deeper, the instability of the keyhole morphology reduces the surface uniformity and compromises the densification. Furthermore, this finding confirms that keyhole formation can initiate also in a transition melting regime at high laser power-speed conditions [22], which can be bound approximatively into the 100–167 J/mm³ VED range for IN625. Considering the transition regime, the results prove to be consistent with the optimal VED range of 60–100 J/mm^3 for IN625 densification by PBF-LB [10].

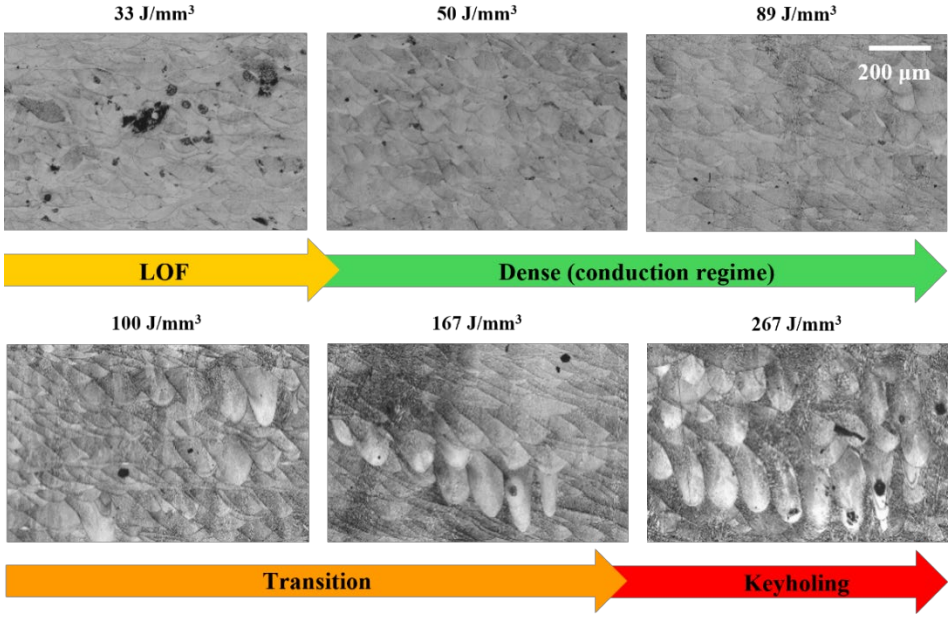

Fig. 6. OM of etched cross-sections of IN625 samples showing the progressive evolution of melt pool morphology toward keyholing.

To further clarify the comparison between the *P–v* and the *VED*-based approaches, Fig. 7 illustrates the laser power–speed domain with superimposed volumetric energy density contours. The yellow region defines the optimal *P–v* window for the robust and simultaneous optimization of surface roughness, microhardness, and relative density, corresponding to a narrow scan speed interval of approximately 1000 mm/s at laser powers exceeding 100 W. The blue band highlights the range of *VED* associated with the same multi-property optimization, approximately covering the 89–167 J/mm³ range. Notably, the limited overlap between the two areas indicates that relying only on *VED* would encompass *P–v* combinations associated with reduced process stability and non-optimal melt pool behavior. These findings are consistent with recent literature on PBF-LB, which has highlighted that identical *VED* values can correspond to markedly different melt pool morphologies and stability conditions owing to the distinct and non-linear influence of laser power and scan speed on melt pool dynamics and molten metal flow [23–25]. These observations confirm that while useful for trend identification and comparison with literature, *VED* is insufficient as a primary variable for PBF-LB process optimization. In contrast, investigating the *P–v* parameter space enables both effective process optimization and a clearer identification of the underlying melting regimes and defect-formation mechanisms.

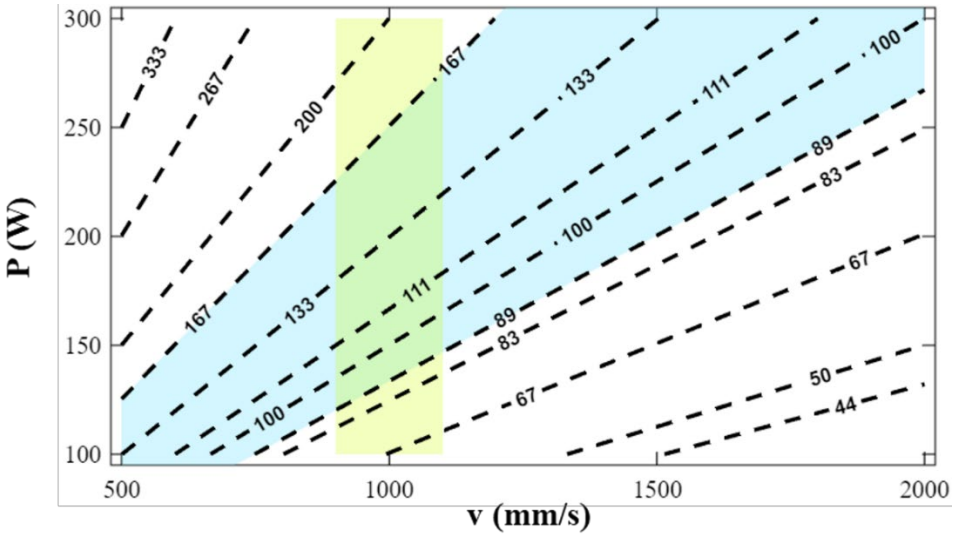

Fig. 7. Process map in the *P*–*v* space with VED contours highlighting the difference between the two optimization approaches.

Conclusion

Through the experimental exploration of a wide *P*–*v* process space for PBF-LB of IN625, this study provides a quantitative identification of the stability domains governing melt-pool behaviour and resulting as-built part quality in terms of surface roughness, microhardness, and density (summarized in Table 2). The study also confirms the intrinsic limitations of *VED* as a primary optimisation parameter for PBF-LB. While *VED* can still delineate energetic windows for post-process interpretation, it lacks the intrinsic capability to robustly define the stability process domain.

Table 2. Optimum ranges of *P*-*v* and *VED* for the properties of IN625 processed by PBF-LB.

Properties	Optimum *P*–*v*	Optimum *VED*	Remarks
Surface roughness	More than 100 W 500–1000 mm/s	More than 89 J/mm³	Sa ≤ 10 µm Stable melt tracks
Microhardness	More than 100 W 500–2000 mm/s	50–267 J/mm³	~300 HV_1 Microstructure refinement
Relative density	More than 100 W 1000–1500 mm/s	67–167 J/mm³	$\rho_{rel} \geq 99.5$ % Transition regime included
Multi-objective	More than 100 W ~1000 mm/s	89–167 J/mm³	Narrow optimal window to achieve balanced properties Attention ought to be paid to transition regime

The main findings of the study can be summarised as follows:

- Surface roughness is the most challenging part property to optimise in-process. Unlike density and microhardness, achieving significant reductions in Sa require operating closer to the transition and keyhole regimes.
- Stable microhardness was achieved across a wide process space that extends near the onset of keyhole formation. This finding suggests that IN625 parts may also exhibit satisfactory tensile strength over a broad process interval.
- Near full-densification was achieved in a broad stability zone where melt-pool consolidation is robust and consistent. Nonetheless, particular attention ought to be paid to the transition melting regime due to the increased risk of keyholing.

Overall, the present study offers new insights to guide future process optimization aimed to deepen the understanding of the trade-offs between surface integrity, densification stability, and mechanical performance in PBF-LB of IN625. Specifically, the structured *P*–*v* mapping offers a valuable

empirical basis for developing data-driven or physics-informed models, especially for multi-objective optimization problems. Besides the need for synthetic energy input indicators that better capture melt-pool dynamics, the findings further suggest the importance of future tensile and fatigue investigations across the identified process domain.

Funding

This study was carried out within the MICS (Made in Italy - Circular and Sustainable) Extended Partnership and received funding from the European Union Next-GenerationEU (PIANO NAZIONALE DI RIPRESA E RESILIENZA (PNRR) – MISSIONE 4 COMPONENTE 2, INVESTIMENTO 1.3 – D.D. 1551.11-10-2022, PE00000004). This manuscript reflects only the authors' views and opinions, neither the European Union nor the European Commission can be considered responsible for them.

References

[1] A. Nowotnik, Nickel-Based Superalloys, in: Reference Module in Materials Science and Materials Engineering, Elsevier, 2016.

[2] T. Islam, B. Zhao, D. Piccone, R. Bertelsen, D. Lin, Z. (Andy) Fan, J. Klemm-Toole, S. Pan, A holistic corrosion understanding in IN625 alloy based on additive manufacturing history and microstructure modification, Electrochim. Acta, 535 (2025) 146697.

[3] J.M. Rakowski, C.P. Stinner, The Use and Performance of Wrought 625 Alloy in Primary Surface Recuperators for Gas Turbine Engines, in: CORROSION 2005, NACE International, 2005: pp. 1–14.

[4] Z. Tian, C. Zhang, D. Wang, W. Liu, X. Fang, D. Wellmann, Y. Zhao, Y. Tian, A Review on Laser Powder Bed Fusion of Inconel 625 Nickel-Based Alloy, Applied Sciences, 10 (2019) 81.

[5] M. Karmuhilan, S. Kumanan, A Review on Additive Manufacturing Processes of Inconel 625, J. Mater. Eng. Perform., 31 (2022) 2583–2592.

[6] M.C. Karia, M.A. Popat, K.B. Sangani, Selective laser melting of Inconel super alloy-a review, in: 2017: p. 020013.

[7] M.A. Buhairi, F.M. Foudzi, F.I. Jamhari, A.B. Sulong, N.A.M. Radzuan, N. Muhamad, I.F. Mohamed, A.H. Azman, W.S.W. Harun, M.S.H. Al-Furjan, Review on volumetric energy density: influence on morphology and mechanical properties of Ti6Al4V manufactured via laser powder bed fusion, Progress in Additive Manufacturing, 8 (2023) 265–283.

[8] K. Mumtaz, N. Hopkinson, Top surface and side roughness of Inconel 625 parts processed using selective laser melting, Rapid Prototyp. J., 15 (2009) 96–103.

[9] R. Sheshadri, M. Nagaraj, A. Lakshmikanthan, M.P.G. Chandrashekarappa, D.Y. Pimenov, K. Giasin, R.V.S. Prasad, S. Wojciechowski, Experimental investigation of selective laser melting parameters for higher surface quality and microhardness properties: taguchi and super ranking concept approaches, Journal of Materials Research and Technology, 14 (2021) 2586–2600.

[10] M.J. Benoit, M. Mazur, M.A. Easton, M. Brandt, Effect of alloy composition and laser powder bed fusion parameters on the defect formation and mechanical properties of Inconel 625, The International Journal of Advanced Manufacturing Technology, 114 (2021) 915–927.

[11] A. Paraschiv, G. Matache, M.R. Condruz, T.F. Frigioescu, L. Pambaguian, Laser Powder Bed Fusion Process Parameters' Optimization for Fabrication of Dense IN 625, Materials, 15 (2022) 5777.

[12] J.-R. Poulin, A. Kreitcberg, P. Terriault, V. Brailovski, Long fatigue crack propagation behavior of laser powder bed-fused inconel 625 with intentionally-seeded porosity, Int. J. Fatigue, 127 (2019) 144–156.

[13] H. Yeung, F.H. Kim, M.A. Donmez, J. Neira, Keyhole pores reduction in laser powder bed fusion additive manufacturing of nickel alloy 625, Int. J. Mach. Tools Manuf., 183 (2022) 103957.

[14] R. Yamanoglu, Effect of laser energy density on porosity and microstructural features of Inconel 625 alloy produced by selective laser melting, Journal of Advances in Manufacturing Engineering, (2024) 84–93.

[15] A. Shahrjerdi, M. Karamimoghadam, R. Shahrjerdi, G. Casalino, M. Bodaghi, Optimizing Selective Laser Melting of Inconel 625 Superalloy through Statistical Analysis of Surface and Volumetric Defects, Designs (Basel)., 8 (2024) 87.

[16] R.A. Yildiz, O. Gokcekaya, M. Malekan, A holistic analysis of laser powder bed fusion process parameters for Inconel 625 superalloy: microstructural features and mechanical performance, Progress in Additive Manufacturing, (2025).

[17] M.A. Balbaa, M.A. Elbestawi, J. McIsaac, An experimental investigation of surface integrity in selective laser melting of Inconel 625, The International Journal of Advanced Manufacturing Technology, 104 (2019) 3511–3529.

[18] C. Guo, S. Li, S. Shi, X. Li, X. Hu, Q. Zhu, R.M. Ward, Effect of processing parameters on surface roughness, porosity and cracking of as-built IN738LC parts fabricated by laser powder bed fusion, J. Mater. Process. Technol., 285 (2020) 116788.

[19] S. Li, Q. Wei, Y. Shi, Z. Zhu, D. Zhang, Microstructure Characteristics of Inconel 625 Superalloy Manufactured by Selective Laser Melting, J. Mater. Sci. Technol., 31 (2015) 946–952.

[20] H.R. Javidrad, S. Salemi, Effect of the Volume Energy Density and Heat Treatment on the Defect, Microstructure, and Hardness of L-PBF Inconel 625, Metallurgical and Materials Transactions A, 51 (2020) 5880–5891.

[21] M. Giovagnoli, G. Silvi, M. Merlin, M.T. Di Giovanni, Optimisation of process parameters for an additively manufactured AlSi10Mg alloy: Limitations of the energy density-based approach on porosity and mechanical properties estimation, Materials Science and Engineering: A, 802 (2021) 140613.

[22] Y. Huang, T.G. Fleming, S.J. Clark, S. Marussi, K. Fezzaa, J. Thiyagalingam, C.L.A. Leung, P.D. Lee, Keyhole fluctuation and pore formation mechanisms during laser powder bed fusion additive manufacturing, Nat. Commun., 13 (2022) 1170.

[23] G.V. de Leon Nope, L.I. Perez-Andrade, J. Corona-Castuera, D.G. Espinosa-Arbelaez, J. Muñoz-Saldaña, J.M. Alvarado-Orozco, Study of volumetric energy density limitations on the IN718 mesostructure and microstructure in laser powder bed fusion process, J. Manuf. Process., 64 (2021) 1261–1272.

[24] R. Zhao, C. Chen, W. Wang, T. Cao, S. Shuai, S. Xu, T. Hu, H. Liao, J. Wang, Z. Ren, On the role of volumetric energy density in the microstructure and mechanical properties of laser powder bed fusion Ti-6Al-4V alloy, Addit. Manuf., 51 (2022) 102605.

[25] C. Smith, G. Hommer, M. Keeler, J. Gockel, K. Findley, C. Brice, A. Clarke, J. Klemm-Toole, Assessing Volumetric Energy Density as a Predictor of Defects in Laser Powder Bed Fusion 316L Stainless Steel, JOM, 77 (2025) 737–748.